UNIVERSIDAD DE CANTABRIA

Facultad de Ciencias

Departamento de Física Aplicada

Tesis Doctoral

SYNTHESIS, STRUCTURAL CHARACTERIZATION AND SPECTROSCOPIC STUDY OF NANOCRYSTALLINE AND MICROCRYSTALLINE MATERIALS

Rosa Martín Rodríguez

Santander, Noviembre de 2010

Chapter 4

Experimental Methods

4.1 Introduction

Along this chapter, we show the experimental procedures and equipment utilized not only for the structural characterization of the samples, but also for the spectroscopic study developed. First, XRD and transmission electron microscopy (TEM) techniques are detailed. Then, the different setups used for the spectroscopic measurements are described. Absorption, luminescence, excitation, lifetime and Raman measurements have been performed. Besides, low temperature and high pressure techniques are described. Finally, the spectra correction procedures are explained.

4.2 Structural characterization

Different techniques such as XRD or TEM were employed to characterize the prepared materials. XRD measurements were accomplished in order to check the phase purity of all samples and to estimate the particle size in the case of nanocrystalline samples. Average particle size and size distribution of the nanoparticles were also estimated from TEM images.

4.2.1 X-ray diffraction

XRD technique is commonly applied for the structural characterization of all kind of materials. It is based on the diffraction produced when a X-ray beam is scattered by a material. If the material presents crystalline structure, the scattered waves interfere in a

constructive way for specific directions according to Bragg's law, $2d\sin\theta = n\lambda$, where d is the distance between crystallographic planes, λ is the incident X-ray wavelength, θ is the angle between the incident wave and the dispersion plane, and n is an integer number indicating the diffraction order.

Various X-ray diffractometers were used to obtain XRD patterns (see Fig. 4.1). A Philips 1700 diffractometer with a Bragg-Brentano $\theta - 2\theta$ geometry, in which the X-ray source is fixed, the sample turns θ and the detector turns 2θ, was utilized at the Solid State Physics laboratory (University of Cantabria). A Thermo Electron ARL X'TRA based on a vertical $\theta - \theta$ geometry, where both the X-ray source and the detector move an angle θ, was employed during a collaboration with Prof. Marco Bettinelli at the Biotecnology Department (University of Verona). Both diffractometers are equipped with a Cu-anode X-ray source (K_α, λ=1.5418 Å). The phase of the samples synthesized at Verona was identified by comparing the obtained XRD patterns with the PDF 4+ 2006 database and using SIeve program, while MAUD program was used for Rietveld data refinement [1].

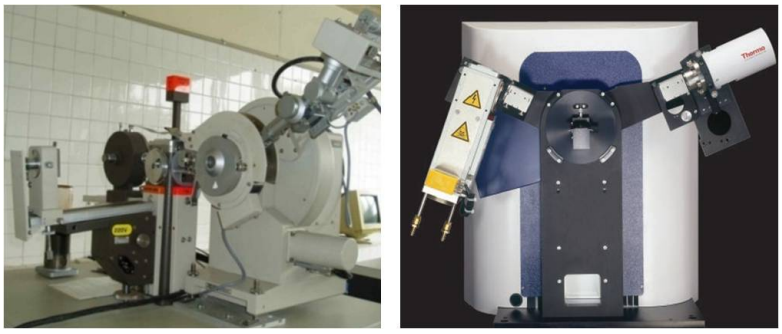

Figure 4.1: X-Ray diffractometers employed to characterize our samples, Philips 1700 (left) and Thermo Electron ARL X'TRA (right).

High pressure XRD experiments were developed with a Xcalibur diffractometer (Oxford Diffraction Limited) (Fig. 4.2) at the Complutense University of Madrid within the MALTA-Consolider project. XRD patterns were obtained on a 135 mm Atlas charge-coupled device (CCD) detector placed at a distance of 90 mm from the sample using $K_{\alpha1}$: $K_{\alpha2}$ molybdenum radiation (λ=0.7107 Å). The X-ray beam was collimated to a diameter of 300 μm. Exposure times were generally of 1 hour and the accessible angular range is 4θ=60°. The observed intensities were integrated as a function of 2θ in order to give conventional one-dimensional diffraction profiles. The CrysAlis software (Oxford

Diffraction Limited) was used for the data collection and the preliminary reduction of the data. The indexing and refinement of the powder patterns were performed using the TOPAS package.

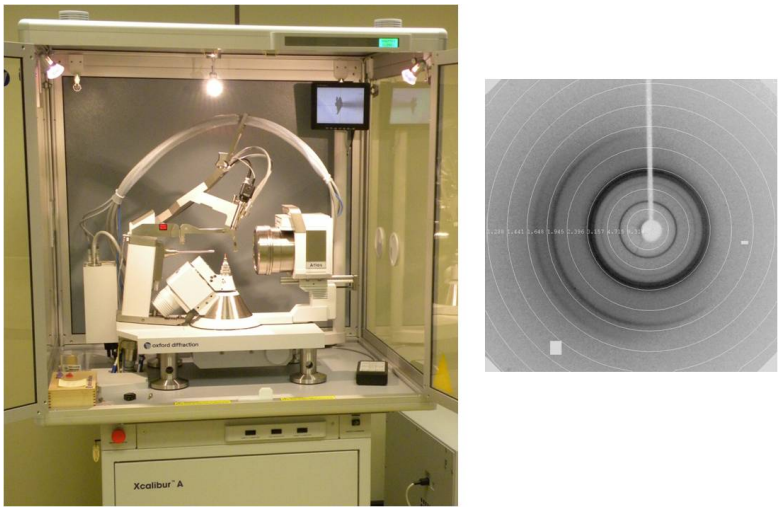

Figure 4.2: Xcalibur diffractometer (Oxford Diffraction Limited) used for the high pressure measurements (left). A CCD image of a CdS XRD pattern under pressure is also shown (right).

The particle size can be determined by X-ray peak broadening analysis for nanocrystalline samples with size up to 500 nm [2]. The peaks diffraction broadening arises mainly due to three factors: Instrumental effects, crystalline size and lattice strains. The peak width due to instrumental broadening is estimated using a standard Si sample. If the observed XRD peak has a width B_0, and the width due to instrumental effects is B_i, then B_r, which corresponds to XRD peak width at half-maximum once the instrumental broadening has been substracted, $B_r = \sqrt{(B_0 - B_i)\sqrt{B_0^2 - B_i^2}}$, is due to both crystalline size and lattice strains. Broadening of XRD peaks due only to crystalline size is given by Scherrer formula, $B_c = \frac{k\lambda}{L\cos\theta}$, where λ is the X-ray wavelength, θ is the Bragg angle, L is the average particle size and k is a constant. The broadening caused by lattice strains can be represented by $B_s = \eta \tan\theta$, where η is the strain in the material. From these expressions, the Williamson-Hall equation to determine the particle size is deduced [3]:

$$B_r = B_c + B_s = \frac{k\lambda}{L\cos\theta} + \eta\tan\theta \rightarrow B_r\cos\theta = \frac{k\lambda}{L} + \eta\sin\theta \tag{4.1}$$

When $B_r\cos\theta$ is plotted against $\sin\theta$ a straight line is obtained; crystalline size can

be calculated from the intercept value $\frac{k\lambda}{L}$ [2]. The Williamson-Hall approach separates the effect of size and strain in the nanocrystals. Spherical shape is assumed for the nanoparticles. Strain contribution to the line broadening is significant for nanoparticles grown by mechanical procedures.

4.2.2 Transmission electron microscopy

TEM is a technique of great importance as far as structural characterization of nanometric systems is concerned. In TEM measurements, electrons are accelerated and focused on the specimen (sample) by the condenser system, usually two lenses. After passing through the sample, electrons are collected and the objective lenses form both images and diffraction patterns. The main parts of the microscope are: Electron source, sample holder, light and electron optics, electron detection and display. The TEM resolution, the smallest distance that can be resolved δ, is given by $\delta = \frac{0.61\lambda}{\beta}$, where λ is the wavelength of the radiation and depends on the electrons energy, and β is the semi-angle of collection of the magnifying lenses. One important drawback of the TEM is that only a small part of the sample is seen at a time. Moreover, TEM presents 2D images of 3D specimens, so the information is averaged through its thickness. Another limitation is related to the fact that samples must be "electron transparent", which means they must be thinner than 100 nm. For our powder specimen, preparation is easier than for thin films or metallic samples, and involves selecting fine powder, suspending it in a non reactive liquid, and placing it on the grid [4].

TEM experiments were performed on a JEM 2100 electron microscope (JEOL, Japan) (Fig. 4.3) at the TEM facility at the University of Cantabria (SERMET), operating at an accelerating voltage of 200 kV, with an estimated point to point resolution of 0.23 nm, and equipped with a CCD detector (Gatan *Orius SC 1000B*). DigitalMicrograph (Gatan) software was employed for the data collection and treatment. The samples were prepared by suspending the solid powder in ethanol (Panreac, 96 purity) under ultrasonic vibration. One drop of the prepared suspension was applied to carbon films on copper grids (Agar Scientific).

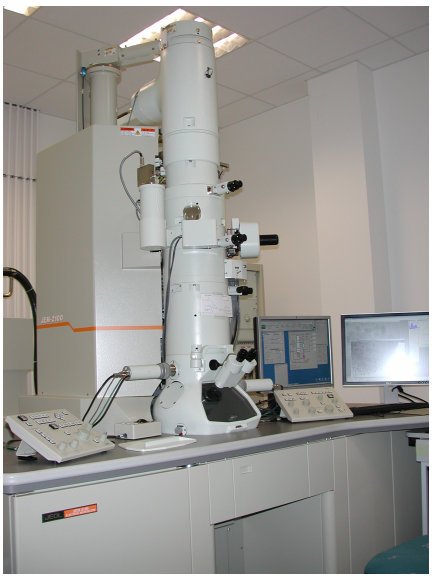

Figure 4.3: JEM 2100 transmission electron microscope (JEOL, Japan) used at the TEM facility at the University of Cantabria.

4.3 Spectroscopy

The aim of this work is the study of the optical properties of the synthesized materials. Different spectroscopic techniques were used to analyze the involved transitions in the light-matter interaction. As it is described below, absorption, luminescence, excitation, time resolved spectroscopy, lifetime and Raman spectroscopy techniques were applied. The spectroscopic measurements were carried out at the High Pressure and Spectroscopy group laboratories at the University of Cantabria.

4.3.1 Absorption

A light beam becomes attenuated in a material according to *Lambert-Beer* law, $I = I_0 \exp(-\alpha x)$, where I_0 is the incoming intensity, I is the light intensity after passing through a thickness x of the sample, and α is the absorption coefficient. Absorption spectra involve the measurement of the light attenuated by a sample as a function of the radiation wavelength, $A(\lambda)$. The absorbance is defined as $A = \log \frac{I_0}{I}$. In the case of powder materials, absorption can only be measured by using very thin samples, although reflectance spectra provide similar information. The spectral reflectance is defined as the ratio of the flux reflected by the specimen to that of a standard surface under identical

geometrical and spectral conditions. Reflectance spectra can be registered in two different modes: specular reflectance and diffuse reflectance, for the latter, an integrating sphere is required to collect the diffuse reflected light for different wavelengths [5].

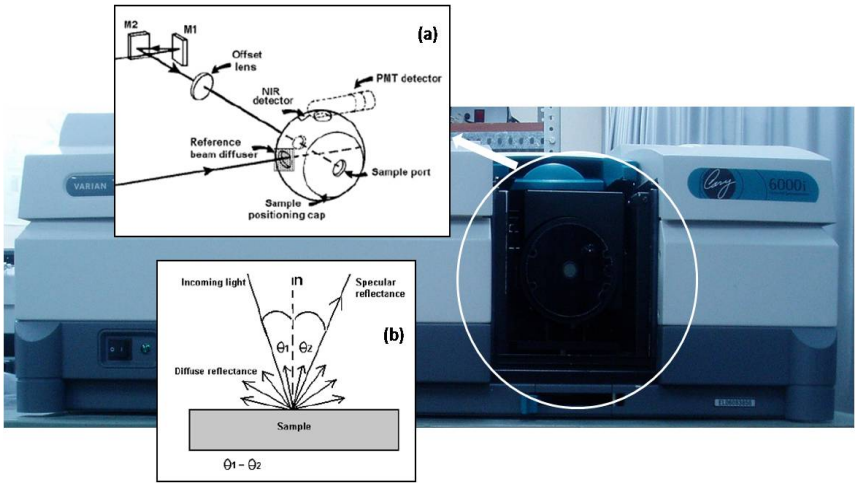

Figure 4.4: Cary 6000i spectrophotometer employed for reflectance measurements. The optical design of the diffuse reflectance sphere (a) and the two components of the reflected light, specular and diffuse reflection (b) are shown.

A Cary 6000i (Varian) spectrophotometer was used to register diffuse reflectance spectra in the range 200-1800 nm (Fig. 4.4). It is equipped with two light sources; a quartz halogen lamp for the visible/IR region and a deuterium lamp for the UV, and two detectors; one photomultiplier (PMT) (Hamamatsu *R928*) for the visible region and one InGaAs detector for the near IR. Diffuse reflectance measurements were performed using a polytetrafluoroethylene (PTFE)-coated integrating sphere. Initially, a baseline is recorded with the PTFE reference disk covering the reflectance port. The sample is then mounted over the port and the light reflected by the sample surface is collected by the sphere. The total (diffuse and specular) or the diffuse-only reflectance (see Fig. 4.4(b)) may be measured by mounting the sample against the sphere port in two different configurations.

A FT-IR System 2000 (Perkin-Elmer) spectrophotometer was used to obtain the transmission spectra in the IR region. It consists essentially of three components: Two radiation sources to cover the 4400-400 cm^{-1} range, one Michelson interferometer and a Mercury-Cadmium-Telluric detector. In addition, IR absorption spectra of the samples in the form of KBr pellets were recorded on another spectrophotometer (Nicolet *Magna*

760), with a Deuterated-Triglycine-Sulfate detector.

Absorption experiments at high pressure requires non-conventional home-made setups. The experimental apparatus used in this work is shown in Fig. 4.5. Tungsten and deuterium lamps attached to a monochromator (Acton Research Corporation *Spectra Pro-300i*) were used to obtain monochromatic light. One parabolic mirror and two reflection objectives were incorporated in order to avoid chromatic aberration. The first objective focuses the excitation beam in the hydrostatic cavity and the second one collects the transmitted light, which is measured using a PMT with a lock-in technique (Stanford Research systems *Sr830 DSP*). A spatial filter must be used before the first objective.

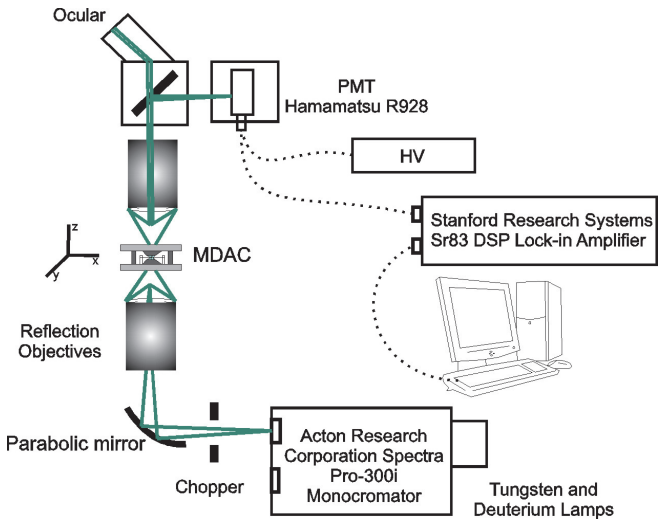

Figure 4.5: Optical setup to measure high pressure absorption at the High Pressure and Spectroscopy group laboratories, University of Cantabria.

4.3.2 Luminescence and excitation

In luminescence spectra, the emitted light intensity is measured as a function of the wavelength for a fixed excitation wavelength, $I(\lambda)$. On the contrary, in excitation technique, only one wavelength is detected and the excitation wavelength is scanned in a certain spectral range. Both luminescence and excitation, in contrast to absorption, are selective techniques. Different light sources in the IR-visible-UV range, diverse detection systems sensitive to those spectral regions and several monochromators were used to obtain this kind of spectra. All spectra were corrected for the system response and were represented as photons counts vs wavenumbers (see Section 4.6).

A standard spectrofluorimeter (Jobin-Yvon *Fluorolog-2*) was employed for the measurement of photoluminescence and excitation spectra at room temperature (RT) and low temperatures (Fig. 4.6). The sample is excited with a Xe-lamp followed by an excitation monochromator, and the emitted light is detected with a PMT (Hamamatsu *R928*) at a 90° configuration in order to avoid direct light from the lamp. Continuous wave (CW) UC luminescence spectra were obtained by exciting with a CW laser-diode (LD) (LUMICS GmbH & Arroyo Instruments) and using the *Fluorolog-2* detection system (see setup scheme in Fig 4.6(a)). The LD can reach a maximum output power of 4 W and its emission wavelength can be slightly tuned by changing the temperature. To obtain the spectra, the nanopowders were transferred into a quartz capillary and closed after partial air evacuation. A special sample holder was designed and adapted to the *Fluorolog-2* (Fig. 4.6(b)). This allows to measure all the samples in identical conditions. Yb^{3+} luminescence spectra were recorded by exciting with the LD in a single monochromator equipped with an extended IR PMT (Hamamatsu *R7102*).

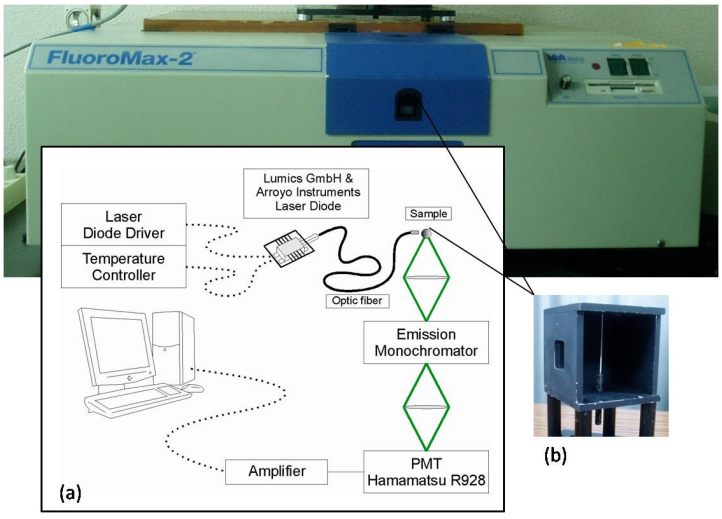

Figure 4.6: Jobin-Yvon *Fluorolog-2* fluorimeter used for luminescence and excitation measurements. The adapted setup for temperature-dependent UC experiments upon excitation with a LD (a) and the sample holder (b) are also shown.

Another setup utilized to obtain luminescence spectra is shown in Fig. 4.7. An optical parametric oscillator (OPO) laser system (Opotek Vibrant model *B 355 II*) pumped by the third harmonic of a Q-switched Nd:YAG (Brilliant Quantel) was used as excitation source. This tunable OPO system offers an approximate pulse width of 10 ns with a

repetition rate of 10 Hz, and a continuous tuning range of 410-710 nm in the visible region (*signal* mode) and 710-2400 in the IR region (*idler* mode). Pulses were guided through a coupled optic fiber to the sample. The emitted light is collected by a 10× Mitutoyo objective and guided through a fiber to the detection system. A monochromator (TRIAX 320) and an intensified CCD camera (Horiba-Jobin-Yvon *iCCD 3553*) were used for the visible and UC luminescence intensity detection.

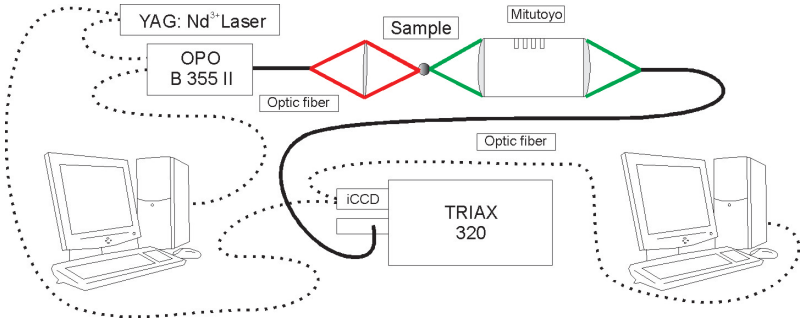

Figure 4.7: Optical setup used for visible and UC luminescence experiments at the High Pressure and Spectroscopy group laboratories, University of Cantabria.

4.3.3 Lifetime and time resolved spectroscopy

To obtain information about both radiative and non-radiative decay from an excited state and energy transfer processes, the luminescence temporal evolution after pulsed excitation must be measured. This was performed in two different manners:

- Recording the temporal dependence of the luminescence intensity at a specific wavelength. For the simplest case, in which excitation and emission occur in the same center, an exponential decay is measured. Fitting this curve to a single exponential, $I(t) = I_0 \exp(\frac{-t}{\tau})$, the excited state lifetime, τ, is obtained. On the contrary, when energy transfer processes are involved, an intensity rise followed by a decay is detected once the excitation pulse has stopped.

- Obtaining the whole emission spectra at different times after the excitation pulse has reached the sample. This experimental procedure is called time-resolved luminescence and the emission spectrum is recorded at a certain delay time with respect to the excitation pulse and within a temporal gate. This technique is very useful to

explore energy transfer processes and allows us to identify contributions of different optically active centers present in a sample if they have different desexcitation dynamics.

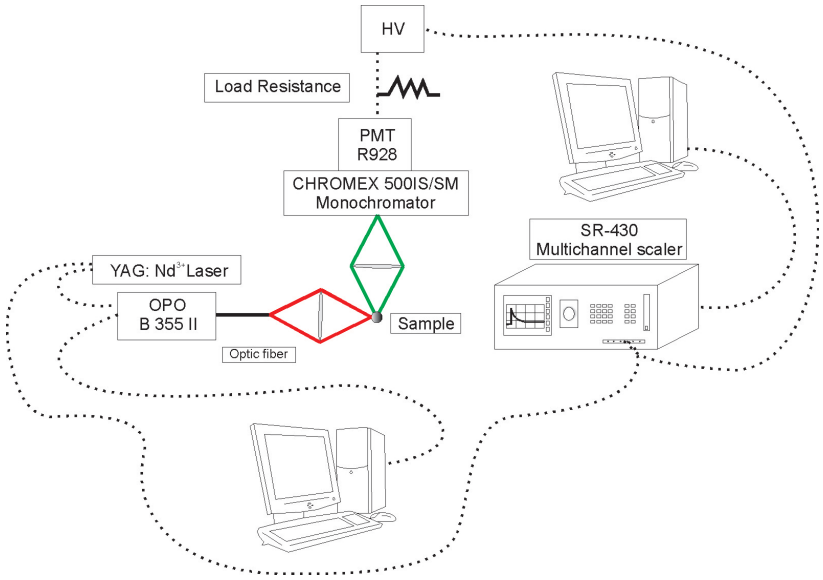

Figure 4.8: Optical setup for lifetime measurements at the High Pressure and Spectroscopy group laboratories, University of Cantabria.

For fluorescence lifetime experiments, the 10 ns laser pulses of the OPO system or modulated LD excitation were used. In the case of this last device, the modulation frequency must be suitable so that the system can reach the steady state and the lifetime can be measured. The setup employed for lifetime measurements upon OPO pulsed excitation is shown in Fig. 4.8. The sample luminescence was dispersed by a 0.50 m single monochromator (CHROMEX 500IS/SM) equipped with 500 nm blazed 1200 grooves/mm and 750 nm blazed 600 grooves/mm gratings, detected by a PMT (Hamamatsu *R928*) or extended IR PMT (Hamamatsu *R7102*) and recorded with a multichannel scaler (Stanford Research SR-430). An appropriate load resistance was placed between both devices. The time constant of the RC circuit ($C = 10\ pF$) should be much lower than the luminescence lifetime, τ, in order to avoid deconvolution processes. The smallest load resistance, $R = 20\ \Omega$ was used in all measurements. The OPO+iCCD setup described in the previous section (fig. 4.7) was also used for lifetime and time-resolved luminescence experiments.

4.3.4 Raman

Raman spectroscopy deals with the study of the fraction of incident light scattered by a sample. Rayleigh scattering is an elastic photon process in which the scattered photon energy is equal to the incident photon energy. However, in Raman spectroscopy the light is inelastically scattered by a substance. The Stokes and anti-Stokes Raman scattering involve virtual levels which do not correspond to real states, as a result, Raman spectra are much weaker than fluorescence spectra by a factor of about $10^6 - 10^8$. Raman experiments are usually carried out under non-resonant illumination so that the Raman spectrum is not masked by the more efficient emission spectrum [5], [6]. A typical Raman spectrum shows an intense band at the incident frequency, ω_0, resulting from Rayleigh scattering, and fainter Raman bands on both sides of ω_0 at distances corresponding to vibrational frequencies, ω_k. In practice, the Stokes Raman scattering is more intense than the anti-Stokes and the lower spectral region is used [7].

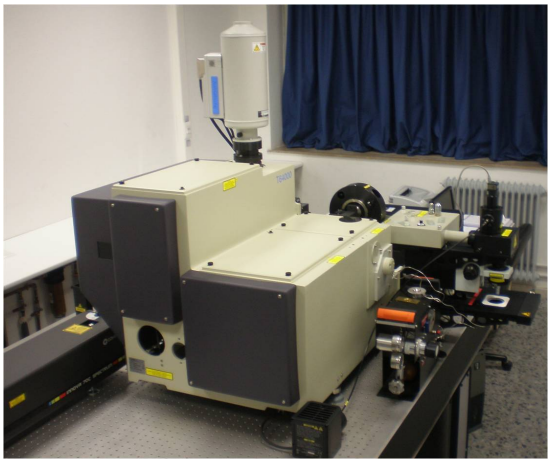

Figure 4.9: Equipment used for Raman measurements at the High Pressure and Spectroscopy group laboratories, University of Cantabria.

The T64000 Raman spectrometer system (Horiba), together with a Kripton-Argon laser (Coherent Innova Spectrum 70C) (the 514.5 nm green line was used), and a Nitrogen cooled CCD (Jobin-Yvon *Symphony*) with a confocal microscopy for the detection (Fig. 4.9), were employed for Raman experiments. The T64000 system is composed of three monochromators (640 mm focal length) with two basic configurations; triple additive mode, with the three monochromators operating in series (3×640 mm focal length),

and substractive mode, in which the two first monochromators filter the laser, and the analysis is done with the third one. Different high pressure cells can be adapted to the XYZ automated stage for high pressure measurements. LabSpec software permits data acquisition and treatment.

4.4 Temperature dependence

Many of the spectroscopic characterization measurements, such as luminescence, excitation or lifetime, were accomplished as a function of temperature.

- Low temperature measurements were achieved using a closed-cycle helium cryostat (Air Products *CS202E*) (Fig. 4.10). The major components are the expander or cold finger, the compressor, the radiation shield and the vacuum shroud. The sample is placed on the cold finger using *Cry-Con* copper-filled thermal grease to fix the sample and to ensure thermal conductivity at low temperatures. This system requires a vacuum pump for the sample space. A combination of a diffusion pump (Leybold *PD 180 L*) with a rotatory pump (Leybold *Trivac B*) as well as a turbomolecular pump (Varian *Turbo Dry 70*) were employed in our experiments. A programmable temperature controller (APD-K cryogenics *HC-2*) together with a Si-diode thermocouple let us modify and stabilize the temperature in the range 10-300 K with an accuracy better than 0.1 K.

Figure 4.10: Closed-cycle helium cryostat components (left) and compressor (right) used for low temperature experiments down to 15 K.

- High temperature experiments (300-650 K) were performed using a microscope heating stage (Leitz 350) (Fig. 4.11). The sample is placed between two quartz films and put into a metallic cavity. The heat is controlled by a rheostat and a thermocouple is used to measure the temperature.

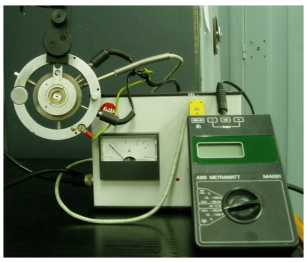

Figure 4.11: Heating stage, power supply and thermometer for the temperature measurements used in the range 300-650 K.

4.5 High pressure measurements

High pressure studies are a valuable mechanism to explore changes in materials as a function of volume without changing the chemical composition. Hydrostatic pressure is used to systematically influence the bonding environment of luminescent centers and therefore modify electronic states energy and transitions probabilities. Sometimes, high pressure can induce structural phase transitions and even stabilize structures not achievable through other means. As a consequence, their optical properties change [8]. High pressure is also a very efficient tool for understanding the electronic structure of semiconductors. The interatomic distance is reduced in average when hydrostatic pressure is applied to a material, and this fact normally causes an increase in the semiconductor bandgap energy [9].

4.5.1 Diamond anvil cells

High pressure measurements were carried out in diamond anvil cells (DACs). The use of diamond has two important advantages over other anvils. Firstly, diamond is the hardest known material and is capable of reaching higher pressures [10]. Secondly, diamond is transparent in a wide frequency range including X-ray and IR-visible range.

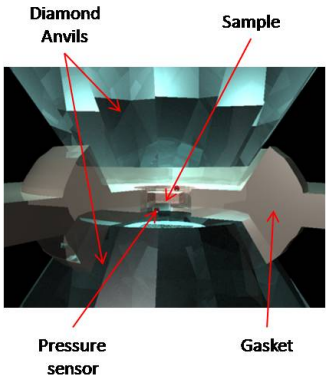

Figure 4.12: Hydrostatic cavity in the cell obtained after placing the perfored gasket containing the sample between the two opposite diamond anvils.

The basic principle of the DAC is very simple. A metal gasket containing the sample, the hydrostatic medium and ruby chips is placed between the flat parallel faces of two diamonds (see Fig. 4.12). By pushing the two opposed anvils together, the sample pressure increases. The gasket is prepared by drilling a hole at the center of the indentation made by the anvil face. Then, the sample, the medium, and a ruby chip if necessary, are placed inside the cavity [11].

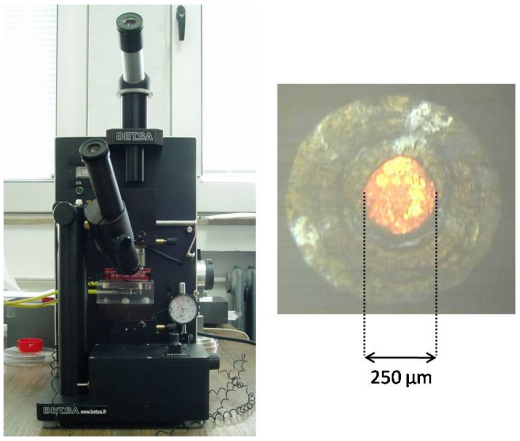

Figure 4.13: Spark eroder used for gaskets perforation. This system allows the utilization of wires between 25 and 400 μm. A picture of a perfored gasket is also shown.

Sample chamber preparation.

The metal foil or gasket serves three purposes; it provides the high-pressure sample chamber, it avoids direct contact between diamonds, and it gives lateral support to the conical faces of the anvils. The gasket is first indented by an anvil face, this process compresses

and hardens the material. The initial thickness of the foil is about 300 μm whereas the indented thickness varies from 50 to 200 μm. The deeper the indentation is, the higher pressures can be reached. Gasket perforation was performed using a semi-automatic spark erosion machine (Betsa *MH*20M) with tungsten electrodes (Fig. 4.13). The hydrostatic cavity diameter was usually between 150 and 300 μm.

DACs specifications.

Different cells were used in the high pressure experiments at the High Pressure and Spectroscopy group laboratories at the University of Cantabria, as well as at the MALTA X-Ray Diffractometer at the Complutense University of Madrid. A Brillouin-Raman cell (Diamond Optics Inc.) (Fig. 4.14) and a Membrane cell (developed at the Pierre and Marie Curie University) (Fig. 4.15) were utilized for absorption and Raman measurements on CdS and ZnO nanocrystals under high pressure. A cryoDAC-Mega cell (easyLab Technologies) was also employed for high pressure luminescence and lifetime experiments on GGG: Cr^{3+} nanoparticles. High pressure XRD measurements on CdS nanocrystals were performed in a modified Merrill-Bassett (MALTA cell).

- **Brillouin-Raman cell** This cell is based on the modification made by Mao and Bell of the Merril-Basset cell, and is designed for reaching pressures as high as 40 GPa [11], [12], [13]. The main body is made of two 440c steel pieces perfectly face to face in which the two plates are fit. Diamond anvils are placed in the middle of the plates. Pressure is applied by turning four allen screws which pull the two plates, and hence the diamonds, together. Type-IIa diamonds with very low luminescent impurities concentration, and with a 0.6 mm culet diameter, were used for the anvil.

- **Membrane cell** The main difference between the membrane cell and the Brillouin-Raman cell is that the former uses a metallic diaphragm or membrane to generate the pressure instead of screws. This cell is composed of two steel parts which fit perfectly one into the other. The membrane, a toroidal cavity in which pressurized gas is introduced, is mounted on the upper part of the cell. When the membrane is inflated, it pushes the upper cylinder against the other increasing the pressure

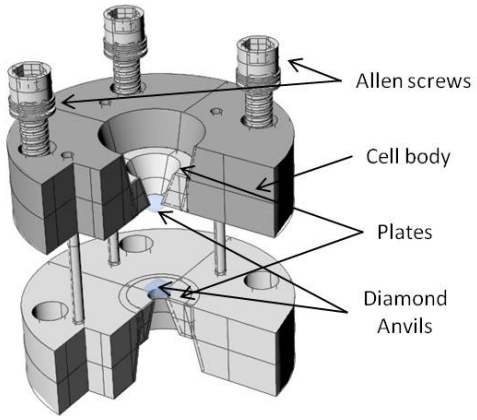

Figure 4.14: Diamond Optics Brillouin-Raman cell used for absorption and Raman measurements at high pressures.

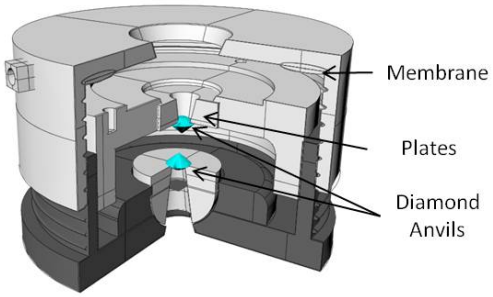

Figure 4.15: Membrane cell used for absorption and Raman measurements at high pressures.

in the hydrostatic cavity. This system allows a fine pressure control and has the advantage that there is no need of moving the cell to change the pressure. The utilized diamond anvils had 0.5 mm of culet size.

- **cryoDAC-Mega cell** This cell, made of CuBe alloy, is suitable for both optical and XRD studies at cryogenic temperatures. The diamond anvils are mounted within CuBe rings and mechanically fixed to their tungsten carbide support plates. The DAC itself is held within two CuBe clamps, and one of them is fixed to the cryostat. Pressure is applied by turning the four bolts on the CuBe blocks.

- **MALTA cell.** In the case of this modified Merrill-Bassett DAC, three screws pull the two plates together [11]. The used diamond anvils had 1 mm of culet size.

4.5.2 Pressure calibration and transmitting media

The most commonly used technique to determine the pressure inside the DAC cavity is based on the pressure shift of the R-lines ($^2E \rightarrow {}^4A_2$) ruby luminescence. The RT R_1 and R_2 shift rate is linear up to 20 GPa according to [14]:

$$\begin{aligned} E_{R_1}(\mathrm{cm}^{-1}) &= 14405 - 7.53 \cdot P(\mathrm{GPa}) \\ E_{R_2}(\mathrm{cm}^{-1}) &= 14434 - 7.53 \cdot P(\mathrm{GPa}) \end{aligned} \tag{4.2}$$

Ruby shows a sharp and efficient luminescence facilitating its detection. However, there are times, like for instance in the case of GGG: Cr^{3+}, when ruby emission can hide the sample luminescence, and a non-luminescent pressure sensor must be used. Spectral shift of Raman lines in diamond have also been calibrated as a function of pressure [15]. The Raman-active phonon energy is $D_R = 1332.26$ cm^{-1} at ambient pressure (AP). Pressure can be expressed as a function of the Raman peak position [16]:

$$D_R(\mathrm{cm}^{-1}) = 1332.26 + 2.64 \cdot P(\mathrm{GPa}) \tag{4.3}$$

The function of the transmitting medium is to ensure a homogeneous pressure distribution in the sample chamber. Pressure gradients and stress must be reduced, since they can alter the physical state of the sample independently of any hydrostatic pressure effects. Basic requirements for the hydrostatic medium are being transparent in the wavelength range under study, and keeping the hydrostaticity within a wide pressure interval. Different transmitting media were used. Paraffin oil is hydrostatic below 10 GPa and it was chosen as a good candidate because it is inert. When higher pressures were required, silicon oil (Dow Corning) was employed. A 4:1 mixture of ethanol: methanol provides hydrostatic conditions at RT up to 10 GPa and it was also used.

4.6 Spectra correction

The correction of the experimental excitation and luminescence spectra is important when precise information about spectral positions, bands shape and intensity is desired. Two

types of corrections were applied in this work.

4.6.1 Wavelength correction

In the spectra shown in this work, the x axis is represented as wavenumbers, in cm^{-1} units. However, the raw data were obtained as a function of wavelength, λ_{air}(nm). To accomplish this conversion, first, we need to calibrate the monochromator using a Hg lamp. Then, the refractive index of air must be considered in order to get the vacuum wavelength, λ_{vac}(nm), according to the following expression [17]:

$$\lambda_{vac} = \lambda_{air} + 2.72643 \cdot 10^{-4} \cdot \lambda_{air} + \frac{1.2288}{\lambda_{air}} + \frac{3.555 \cdot 10^4}{\lambda_{air}^3} \tag{4.4}$$

Finally, the vacuum wavelength, λ_{vac}(nm), is converted into wavenumbers, $E(cm^{-1})$:

$$E(cm^{-1}) = 10^7 \cdot \lambda_{vac}^{-1}(nm) \tag{4.5}$$

4.6.2 Intensity correction

- **Excitation spectra.** In order to correct the excitation spectra intensity, we must bear in mind the different radiation source power as a function of the wavelength, the response $R(\lambda)$. The excitation spectra in the visible region were achieved using a Xe-lamp in the *Fluorolog-2*. The lamp power is measured simultaneously while a spectrum is being collected. Yb^{3+} excitation spectra were recorded exciting with the OPO laser. The laser power is monitored using a beam splitter and a powermeter (Ophir $3A$-SH). In all cases, the excitation spectra were corrected by dividing them by the corresponding response.

- **Emission spectra.** When luminescence spectra are measured, the detector signal is determined by the amount of light emitted by the sample at each wavelength, and the efficiency with which that light is detected. The experimental spectra must be corrected so that they can be interpreted only in terms of the intrinsic emission of the sample. The experimental procedure described by Ejder was followed [18]. The signal can be expressed in terms of I(energy per second) or J(photons per second) for y axis, and either λ(nm) or E(cm^{-1}) for x axis. In this work, all the spectra are

represented as photons vs wavenumbers, so the integrated intensity of an emission band is proportional to the number of emitted photons per time unit. First, the spectrum of a black body source (calibrated filament lamp) was measured at the same experimental conditions, $B(\lambda)$. Then, the lamp spectrum was divided by the theoretical output of the lamp, $J(E)$:

$$J(E) \propto E^2 \frac{1}{\exp(\frac{E}{k_B T}) - 1} \tag{4.6}$$

where T is the black body temperature (2535 K), and the detection system response was obtained, R:

$$R = \frac{B(E)}{J(E)} \tag{4.7}$$

To correct a luminescence spectrum initially expressed in $J(\lambda)$, LS(nm), one must multiply by λ^2(nm), LS'(nm)=LS(nm)$\cdot\lambda^2$(nm), convert x axis to wavenumbers, $LS(\mathrm{cm}^{-1})$ and divide by the response curve, R. The corrected emission spectrum is given by LS_c:

$$LS_c = \frac{LS(\mathrm{cm}^{-1})}{R} \tag{4.8}$$

Bibliography

[1] L. Luterotti and S. Gialanella. X-ray diffraction characterization of heavily deformed metallic specimens. *Acta. Mater.*, **46**: 101–110, 1998.

[2] C. Suryanarayana and M.G. Norton, editors. *X-Ray Diffraction: A Practical Approach*. Plenum Press, New York, 1998.

[3] G.K Williamson and W.H Hall. X-ray line broadening from filed aluminium and wolfram. *Acta. Metall.*, **1**: 22–31, 1953.

[4] D.B. Williams and C.B. Carter, editors. *Transmission Electron Microscopy*. Plenum Press, New York, 1996.

[5] J. García Solé, L.E. Bausá, and D. Jaque, editors. *An Introduction to the Optical Spectroscopy of Inorganic Solids*. John Wiley and Sons Ltd, England, 2005.

[6] B. Henderson and G.F. Imbusch, editors. *Optical Spectroscopy of Inorganic Solids*. Clarendon Press, Oxford, 1989.

[7] E.I. Solomon and A.B.P. Lever, editors. *Inorganic Electronic Structure and Spectroscopy*, volume I. John Wiley and Sons, New York, 1999.

[8] K.L. Bray, editor. *High pressure probes of electronic structure and luminescence properties of transition metal and lanthanides systems*, volume 213 of *Topic in Current Chemistry*. Spring-Verlag, Berlin, 2001.

[9] T. Suski and W. Paul, editors. *Semiconductors and Semimetals*, volume 54 of *High Pressure in Semiconductor Physics I*. Academic Press, San Diego, 1998.

[10] I.V. Aleksandrov, A.F. Goncharov, A.N. Zisman, and S.M. Stishov. Diamond at high pressures: Raman scattering of light, equation of state, and high pressure scale. *Sov. Phys. JETP*, **66**: 384–390, 1987.

[11] A. Jayaraman. Diamond anvil cell and high-pressure physical investigations. *Reviews of Modern Physics*, **55**: 65–108, 1983.

[12] W.B. Holzapfel and N.S. Isaacs, editors. *High-pressure techniques in Chemistry and Physics*. Oxford University Press, New York, 1997.

[13] W.F. Sherman and A.A. Stadtmuller, editors. *Experimental techniques in high-pressure research*. John Wiley and Sons, New York, 1987.

[14] G.J. Piermarini, S. Block, J.D. Barnett, and R.A. Forman. Calibration of the pressure dependence of the R1 ruby fluorescence line to 195 kbar. *J. Appl. Phys.*, **46**: 2774–2780, 1975.

[15] D. Schiferl, M. Nicol, J.M. Zaug, S.K. Sharma, T.F. Cooney, S.Y. Wang, T.R. Anthony, and J.F. Fleischer. The diamond ^{13}C / ^{12}C isotope raman pressure sensor system for high-temperature/pressure diamond-anvil cells with reactive samples. *J. Appl. Phys.*, **82**: 3256–3265, 1997.

[16] A. Tardieu, F. Cansell, and J.P. Petitet. Pressure and temperature dependence of the first-order Raman mode of diamond. *J. Appl. Phys.*, **68**: 3243–3245, 1990.

[17] D.R. Lide, editor. *Handbook of Chemistry and Physics*. 65th edition. CRC Press, 1983.

[18] E. Ejder. Methods of Representing Emission, Excitation and Photoconductivity Spectra. *J. Opt. Soc. Am.*, **59**: 223–224, 1969.